Experimental Mechanics
DOI 10.1007/s11340-006-9010-z

Strain Measurements of Silicon Dioxide Microspecimens by Digital Imaging Processing

W.N. Sharpe Jr. · J. Pulskamp · D.S. Gianola ·
C. Eberl · R.G. Polcawich · R.J. Thompson

Received: 25 July 2006 / Accepted: 21 September 2006
© Society for Experimental Mechanics 2007

Abstract Silicon dioxide thin film is a common component in electronic devices and in MEMS, but its mechanical properties have rarely been studied. Techniques have been adapted and developed to conduct tensile tests on 1.0 μm thick silicon dioxide specimens that are 100, 150, and 200 μm wide and either 1 or 2 mm long. One end of the specimen remains fastened to the substrate, and the other is glued to a silicon carbide fiber attached to a 30 g load cell mounted on a piezoelectric translation stage. Strain is measured by digital imaging of two gold lines applied to the gage section of the transparent specimen. Twenty-five tests yield a Young's modulus of 60.1±3.4 GPa and a fracture strength of 364±57 MPa.

Keywords Thin films · Tensile testing · Strain measurement · Young's modulus · Silicon dioxide · Fracture strength

Introduction

Silicon dioxide (SiO_2) is an integral part of the integrated circuit and microelectromechanical systems (MEMS) architecture. The ability to thermally grow high quality oxide films coupled with the insulating properties of SiO_2 has spurred the technological advances of the semiconductor industry based on Si processing [1–3]. Important uses for SiO_2 include barriers to diffusion and implantation (e.g., *p–n* junction formation), impurity gettering, and serving as a protective passivation layer [1]. While SiO_2 is not typically used as a structural component, large stresses can develop in the material due to mismatch strains (e.g., differential thermal expansion) between the oxide and its adjacent layers [4]. For accurate design and lifetime prediction, the mechanical behavior of SiO_2 at the size scale in practical use must be evaluated.

Silicon dioxide is transparent, and this presents some new challenges in handling and testing. This paper presents a new method for measuring strain in the gage section of tiny tensile specimens along with extensive measurements of Young's modulus and fracture strength.

The "Background" section is very brief—referring to review works for general testing at this size scale and listing only the initial references pertaining to tensile testing. The specimen shapes and the way the material is produced are then presented. A test system consists of a load application and measurement component along with a strain measurement method. The first is fairly straightforward and only briefly described. The "Strain Measurement" section is longer because it presents the new method. Of course the method is not entirely 'new'; it draws on experience of the authors with applying strain markers on microspecimens and digital imaging techniques that have become common. This test method enables extensive testing (critical for brittle materials at this size scale) and data from 25 tests are presented and discussed. The "Concluding Remarks" compare these silicon dioxide properties with other results and discusses the advantages of this version of digital imaging strain measurement versus the Interferometric Strain/Displacement Gage (ISDG).

W.N. Sharpe Jr. (✉, SEM member) · D.S. Gianola · C. Eberl ·
R.J. Thompson (SEM member)
Department of Mechanical Engineering,
Johns Hopkins University,
Baltimore, MD 21218, USA
e-mail: sharpe@jhu.edu

J. Pulskamp · R.G. Polcawich
Sensors and Electron Devices Directorate,
US Army Research Laboratory,
Adelphi, MD 20783, USA

Background

Measurement of the mechanical properties of thin films used in MEMS is a unique challenge because the specimens should be not only thin, but on the same size scale as used in components and systems. This means that gage sections are not only a few microns or less thick, but have planar dimensions on the order of tens or hundreds of microns. Many test methods have been developed over the past 10 years to test such tiny specimens, and a review article summarizes them as of 2001 [5]. These include tension, bending, membrane, and resonant techniques along with nanoindentation. The authors prefer tension testing because it generates a uniform state of stress and strain and is the common method for bulk materials.

The first issue in tension testing of microspecimens is handling and gripping them. Instead of being able to pick up a specimen and mount it in grips, the various tension testing approaches leave one end of the specimen attached to the substrate upon which it was fabricated and mount that substrate to a fixed grip. The other end may also remain attached to the substrate and mounted on a movable grip, but the two portions of the substrate are cut apart to leave a freestanding tensile specimen [6, 7]. Another approach releases one end of the specimen from the substrate and attaches it to the movable grip. Attachment can be by electrostatic means [8, 9] or adhesives [10, 11]. Force measurement can be accomplished with commercial load cells, so these test methods are very similar in concept to familiar bulk tests. A different approach is to fabricate a long strip of the thin film, leave it attached to the substrate at each end, and push it in the middle to generate uniform tension in the two sides [12]. A third approach integrates the specimen with a load frame, which can be attached to a translation stage to extend it, and conducts the test inside an SEM [13].

Strain measurement is the real challenge here. One needs to measure strain in the gage section of the tensile specimen; strain inferred from overall displacements of the grips can have significant errors and large variations. Unique strain measurement techniques developed especially for microspecimens include digital image correlation [14], in-plane interferometry (the ISDG) [7], AFM imaging [11], and out-of-plane interferometry [12]. The transparent nature of silicon dioxide can create difficulties with optical techniques, and this paper presents a new test method for measuring the stress-strain response of these thin-film specimens.

Young's modulus and strength of silicon dioxide have been measured by various test methods, although measurements of the latter are scarce. Jaccodine and Schlegel [15] published one of the earliest investigations of the Young's modulus of SiO_2 using an inflated "balloon" testing apparatus, much like a bulge test. In a study using thermally grown SiO_2 cantilever beams, Young's modulus was measured by employing a variable frequency oscillator to resonate the beams [16]. Weihs et al. [17] reported values for the modulus of SiO_2 obtained using nanoindentation and cantilever microbeams. Several studies [18, 19] have reported values of Young's modulus via measurement of the thermal stresses in thin films. More recent investigations have measured the elastic constants of silicon dioxide using methods such as nanoindentation [20] and atomic force microscopy [21]. However, none of these measurements are by tensile testing, which is the standard method for determining mechanical properties of structural materials. Tsuchiya and co-workers [22] employed microfabricated tensile geometries to measure tensile strengths of SiO_2 films in both vacuum and air, although no elastic properties were reported. That study also revealed a size effect of the tensile strength: smaller sample dimensions resulted in higher strengths. The test method in a more recent study of silicon dioxide from the same source is similar to this work, but Young's modulus was determined indirectly by differential stiffness methods [23].

Material and Specimens

Handling a specimen that is only a few microns thick and a few millimeters in planar dimensions is a challenge; one cannot simply pick it up and place it in a test machine. This means that one part of the specimen must remain fastened to a substrate that can be handled and another part attached to a mechanism that deforms it and measures forces and the resulting displacements or strains. These silicon dioxide specimens were prepared for use with a testing method developed earlier for tensile testing of polysilicon [9].

A silicon dioxide film nominally one micron thick is deposited uniformly on a single-crystal silicon 4-in diameter wafer. It is then patterned and etched into the shapes of the specimens. Finally, the silicon underneath the film is etched to free up the tensile specimens. Figure 1 provides a CAD drawing of one of the specimens. The left end remains attached to the film on the substrate and transitions into the uniform-width gage section. The large area at the right is the grip end; four anchor straps support it. The gaps surrounding the specimen permit the etch gas to attack the silicon substrate underneath the film, but it does not etch the silicon dioxide. The grip end and the transition region at the fixed end are populated with 10 μm diameter etch holes to permit the gas to penetrate these larger areas.

The silicon wafer is cut into dies that are 5×10 mm containing six specimens with different gage-section dimensions; 1 and 2 mm long by 100, 150, and 200 μm wide. The original purpose of different sizes was to enable

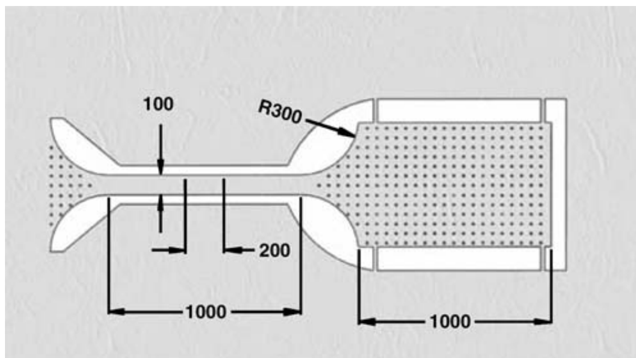

Fig. 1 CAD drawing of the specimen mask for a specimen with a gage length of 1 mm and width of 100 μm. The grip end with etch holes is 0.5×1.0 mm. All shown dimensions are in μm

modulus determination by the differential stiffness method [23], but it also permits study of a potential size effect.

These silicon dioxide films were deposited using plasma enhanced chemical vapor deposition (PECVD) onto silicon (100) substrates using a Plasma-Therm 790 Deposition System. Silane (SiH_4), He, and N_2O were used for the precursors for Si and O, and a deposition rate of approximately 330 Å/min was achieved using a source power of 20 W and maintaining a substrate temperature of 250°C. A post-deposition anneal was employed (AG Associates RTA) for 60 s at 700°C in flowing N_2 to remove any trapped H_2 from the film. The specimen geometry was defined by standard photolithography and then etched with a reactive ion etch (RIE) with CHF_3, CF_4, and He gases at a power of 800 W and with an etch rate of ~750 Å/min. The photoresist was then removed in a Metroline photoresist asher. The specimens were coated with photoresist and the wafer diced. The individual dies were then cleaned in acetone, methanol, IPA, and deionized water. The specimens on the separated dies were released from the silicon substrate in a Xactics xenon difluoride non-plasma etch system. The actual film thickness was measured after the etching process with a Filmetric F200 system to be 0.95±0.005 μm. This system used the reflectance vs. wavelength spectrum to calculate a thickness value for transparent samples. White light was used and the degree to which the reflecting and incident waves were in and out of phase defined the spectrum. The period and amplitude of the resulting signal was a function of the layer thickness and the index of refraction. A function was fit to the raw data to calculate thickness.

Tensile Loading System

The grip end of the specimen is attached to the loading mechanism with a 140 μm diameter silicon carbide fiber—the type used as reinforcements in composites. It is glued to the grip end with Norland NOA 61 ultraviolet-curing adhesive cured by exposure to a handheld cure gun (ThorLabs 560) for 3–6 min. Figure 2 shows a specimen with the fiber glued in place. Silicon dioxide is transparent, so one does not see the specimen in the figure. One sees the fiber, the glue bead, and shadows or reflections from the four anchor straps at the right. What is most visible in the figure is the silicon under the specimen that remains after etching. The area along the gage section is scalloped out by the isotropic gas etch, and one can see the patterns of the etch holes.

Figure 3 is a diagram of the test system. The die containing six specimens is mounted on an aluminum strip attached to a five-axis piezoelectric translation stage (New Focus 8082); this is used to align the axis of the gage section with the fiber. The fiber, approximately 5 cm long, is attached to a 30 g load cell (Transducer Techniques GSO-30) mounted on a single-axis piezoelectric translation stage (New Focus 8302). A capacitance probe (Capacitec 410-SC) monitors the overall displacement of the system.

Strain Measurement

The original intent was to use the ISDG to measure strain in the gage section as was done for polysilicon [7]. The basic concept of the laser-based ISDG uses reflections (actually diffractions) from two tiny, closely spaced markers on a specimen. These create interference patterns that move as the distance between the markers changes. Linear diode arrays sense the intensity of the fringe patterns, and a computer converts their movements into strain on a real-time basis.

Gold markers 200 μm apart and 10 μm wide by 200 μm long were deposited on the gage sections of the silicon dioxide specimens to serve as two ‘points’ for strain measurement. Figure 4 shows two such markers on a transparent specimen. The two brighter vertical lines in the figure are reflections from the bottoms of the scalloped regions in the silicon wafer under the specimen. The edges of the specimen as well as the edges of the film remaining fixed to the wafer are barely visible.

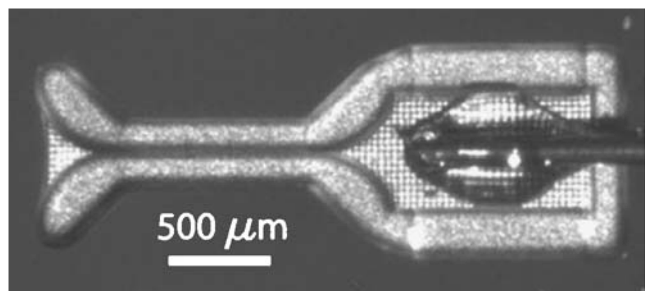

Fig. 2 A silicon carbide fiber glued to the paddle of a transparent silicon dioxide specimen

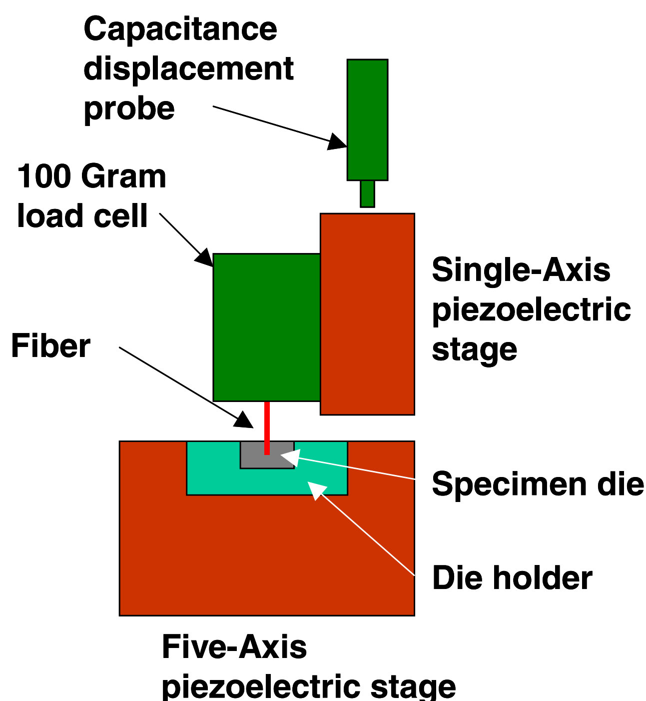

Fig. 3 Schematic of the loading mechanism

Figure 5 shows why the ISDG won't work on these transparent specimens. It is a SEM photo of a cut through the paddle perpendicular to the load axis. The incident laser beam passes through the transparent specimen and is reflected from the scalloped 'trough' generated by isotropic etching in the silicon wafer. Those strong reflections

Fig. 5 SEM photograph of a *cross-section cut* through the specimen paddle after etching

obscure the fringe patterns, which are indeed present but not detectable.

However, if one illuminates the two gold markers at a very oblique angle, they appear as in Fig. 6. The excellent contrast between the markers and the background make a perfect image for digital tracking. A system for Differential Digital Image Tracking (DDIT) was developed, and the setup is shown in Fig. 7.

The test system is mounted on a pneumatic optical table. The light source with its optical fiber guides is shown at left.

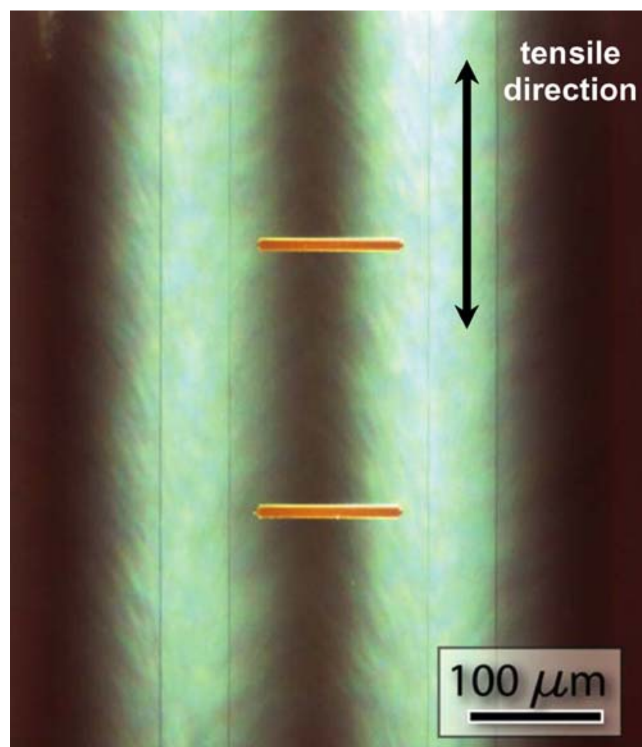

Fig. 4 Two gold markers on a transparent silicon dioxide specimen

Fig. 6 Gold markers with oblique lighting

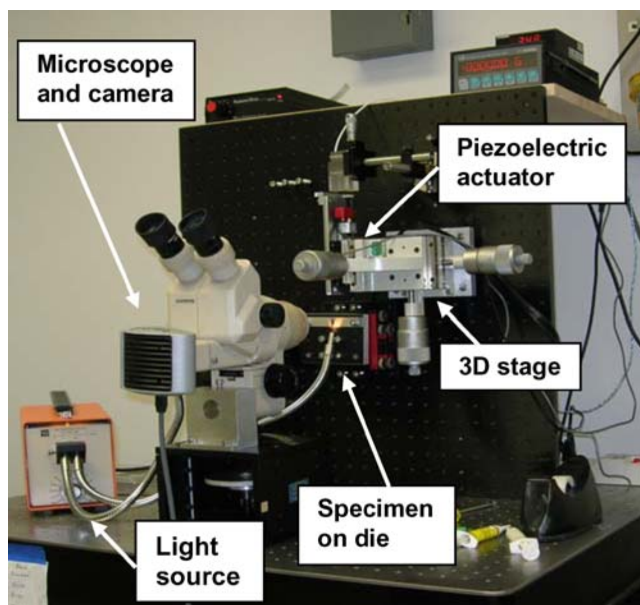

Fig. 7 Overview of DDIT setup

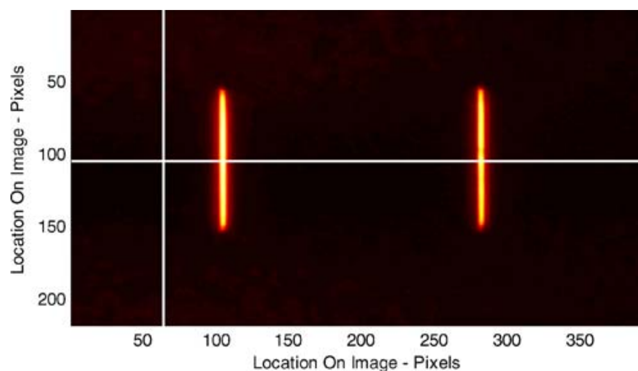

Fig. 8 Intensity plot of two markers showing user-prompt for the location of the line profile

The specimen die and loading mechanism are mounted on a vertical aluminum ‘breadboard’ along with a three-axis manual translation stage for positioning the load-cell mounted fiber with respect to an individual specimen. A 10-63X zoom microscope (Olympus SZ-STB2) is mounted on a vertical stage sitting on the optical table. The camera is a ColorView Soft Imaging System controlled by AnalySIS Imager software on an Athlon 64 3200+ processor with 1 GB of RAM and a FireWire connection.

During loading, sequential digital images are taken through the microscope, saved individually at a rate of approximately one image every 1.3 s, and then processed using Matlab™ once the test is complete. All the saved images are then cropped to enclose only the area around the markers. The post-processing program starts by loading the first image and then prompting the user to choose the area on the image containing the features that are to be tracked. Figure 8 is a screen photo of this first image showing the two markers and a horizontal cursor that is used to select the location on the image (along the tensile axis) that is to be tracked. Next, an averaging width about the selected line (in pixels) is chosen. In Fig. 8 for example, if the tracking line is 100, and an averaging width of 40 pixels is chosen, then an area between 80 and 120 would be tracked on the image.

This now-defined rectangular area is scanned line-by-line horizontally, i.e., collinear with the direction of the specimen’s tensile axis. The pixel intensity scans are averaged and the result is fit with a Gaussian distribution using a least squares algorithm to statistically determine the geometric center of each of the reflective markers on the image. This important averaging step increases the accuracy of the measurement and reduces scatter in the strain data. Figure 9 graphically illustrates the results of this procedure for a typical pair of markers. For each successive image, this fitting procedure is repeated so the motion of these two geometric centers can be compared with the marker centers on the initial image to determine the local engineering strain. Also, as subsequent images are processed, Fig. 9 is continually updated so the user can view the fitting results as they are produced.

The image-processing computer is not equipped for data acquisition, so a separate computer running Agilent VEE software controls the loading of the specimen. This program controls the piezoelectric actuator that pulls the specimen while recording the force and overall displacement. The two programs—loading and image capture—are started and stopped simultaneously. A two-column stress vs. time data file is created on the loading computer and a two-column image number vs. time data file is created on the imaging computer. During post-processing, these two files are compared and then combined automatically based on the commensurate time data columns. For any given test, the stress data acquisition rate is considerably faster than the image acquisition rate so the matching algorithm

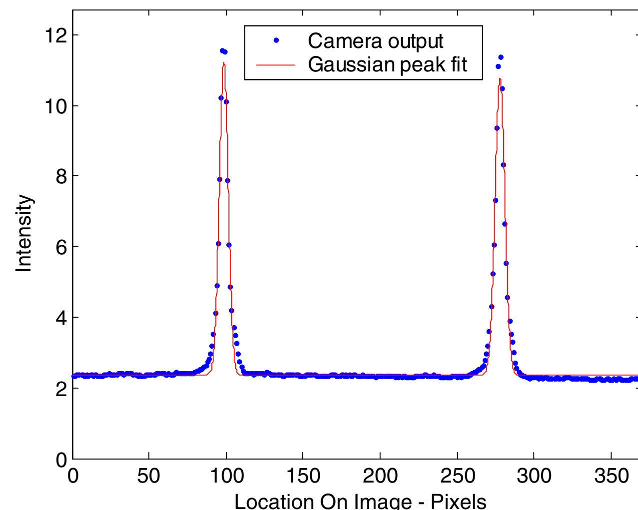

Fig. 9 Measured intensity profile (*points*) along the tensile axis and the Gaussian peak fits (*solid line*) at the two markers

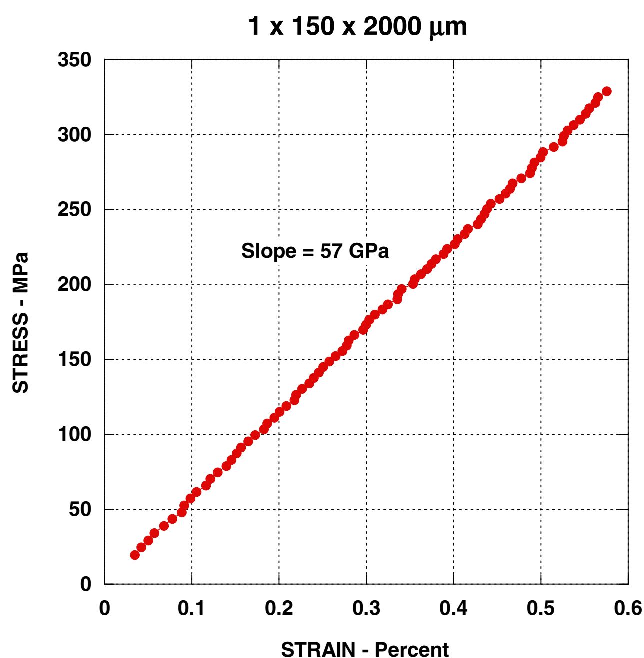

Fig. 10 Representative tensile stress-strain curve for a freestanding SiO_2 thin film specimen

can proceed through each image (and corresponding strain value) to find the stress value that was recorded closest to when the image was taken. Upon completion of the data matching, generation of the stress vs. strain plot is displayed to the user.

A typical stress-strain curve of silicon dioxide is presented in Fig. 10. It is a linear, brittle material as expected, and the plot shows that the test system has good resolution in both stress and strain. Young's modulus is 57 GPa for this sample and the spacing between strain data points is approximately 70 microstrain. One would prefer a finer resolution for stiffer materials such as steel, and this could be obtained by testing at a slower rate. This particular test (86 data points) took approximately 2 min to run and 10 min to process.

Pure rigid body translations were applied to unstrained specimens mounted on a three-axis translation stage to measure the level of uncertainty present using the image-based strain measurement technique. Figure 11 shows the results of the apparent axial strain that was calculated during axial and out-of-plane translations. The zero coordinate of the abscissa represents the position where the markers were approximately centered in the field of view and focused. The sample was moved with the

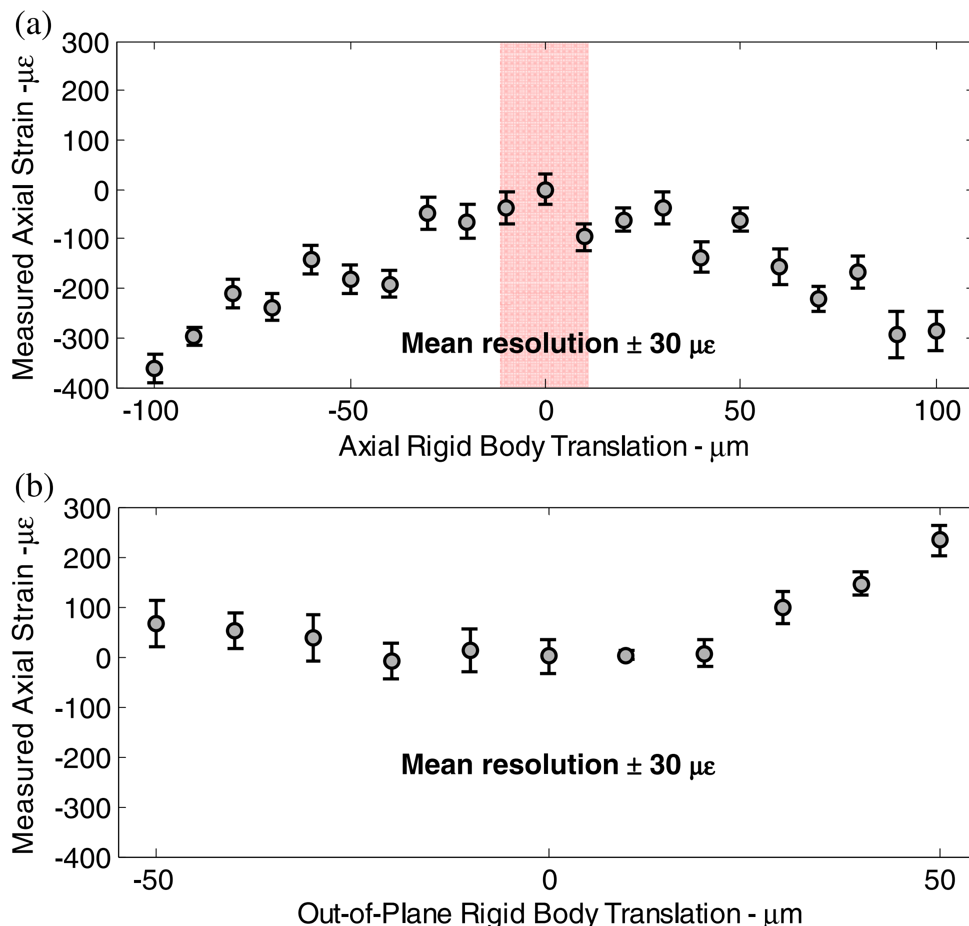

Fig. 11 (**a**) Apparent strain from *axial displacement*. *Shaded area* shows region of typical translations during tensile test. (**b**) Apparent strain from *out-of-plane displacement*

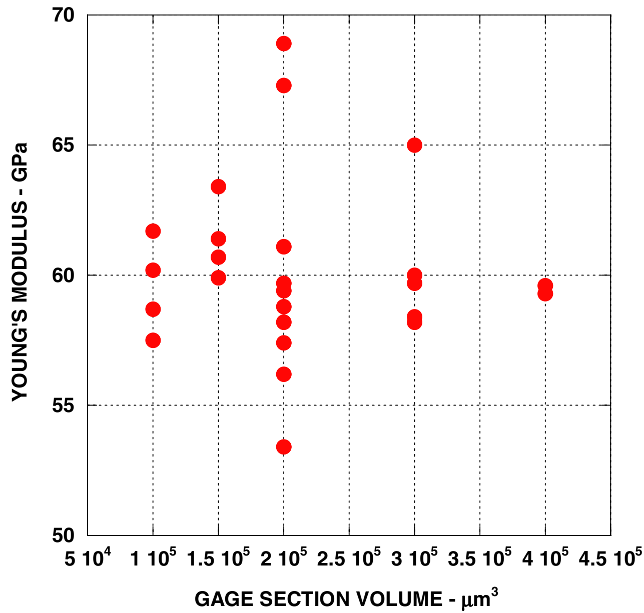

Fig. 12 Modulus versus specimen volume

micrometer-driven stage in increments of 10 μm and each data point represents measurements from ten images taken at each position. The results give an estimate of the resolution (error bars) and error (total strain variation) of this specific optical system and calculation routine.

These experiments yield a mean resolution of ±30 με and ±33 με for axial and out-of-plane translations, respectively, and do not appear to change with relatively large displacements. In contrast, a relatively large error (several hundred με) is incurred if the markers move 100 μm from the optical center. While measuring small elastic strains with this technique would be difficult if large rigid body translations are occurring, the typical total displacements measured for these SiO_2 samples are on the order of ±10 μm [shaded region of Fig. 11(a)] and the corresponding error in this regime is less than 100 με. The resolution of this system could be improved and the error minimized by using a more sophisticated lens system, using a higher-resolution camera, increasing the spacing of two markers, and tracking a larger number of markers.

Results

Test results from such small specimens tend to have a larger scatter simply because of uncertainties in the smaller dimensions, forces, and strain measurements. It is therefore imperative that multiple replications be run. This test setup enables that because of the ease in mounting the specimens and conducting the tests. As many as four tests per day can be conducted and recorded. Fracture strengths of 26 specimens and modulus values of 25 specimens were measured. The strength and modulus values were obtained on the same specimen in all but four cases; occasionally the markers would not be suitable or the specimen would fail early at an obvious flaw. The results, given as mean values and standard deviations, are:

Young's modulus = 60.1 ± 3.4 GPa

Fracture strength = 364 ± 57 MPa

More details are presented in Figs. 12 and 13, which are plots of Young's modulus and fracture strength versus the volume of the specimen gage section. These show the same variations as plots versus surface area since the width is so much larger than the thickness. One would not expect the modulus to vary with specimen size, and Fig. 12 shows that to be the case. However, the question of size effect on strength is always asked, and Fig. 13 reveals a general trend toward higher strengths for smaller specimens. The rationale is that larger specimens of brittle materials can have larger flaws, which lower the strength. It is interesting to note that Fig. 13 looks very similar to Fig. 8 in a 2001 paper [24] on the effect of specimen size on the strength of polysilicon.

The probability of failure, p_f, for uniaxial tensile specimens subjected to a stress, σ, can be described by a Weibull distribution given by:

$$p_f^W = 1 - \exp\left[-\left(\frac{\sigma}{\sigma_\theta}\right)^m\right] \tag{1}$$

where m is the dimensionless Weibull modulus (a larger value of m gives a narrower distribution) and σ_θ is the

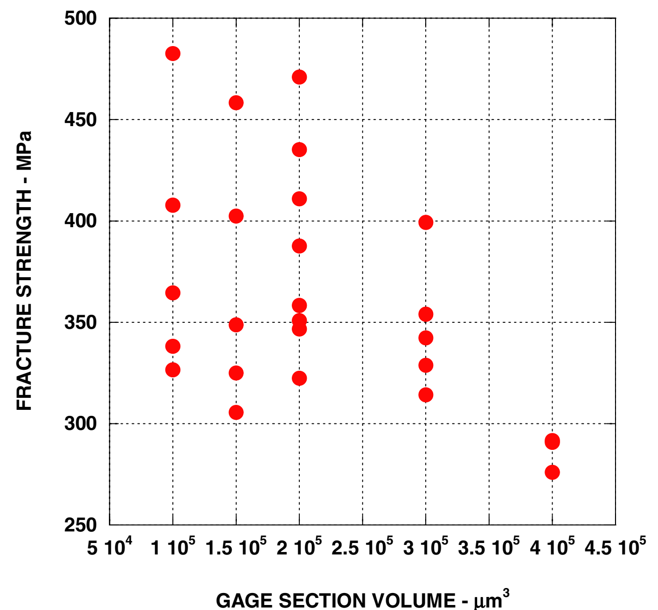

Fig. 13 Strength versus specimen volume

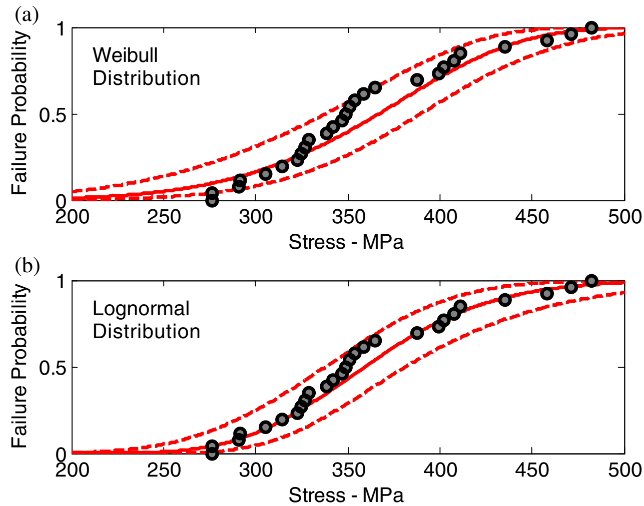

Fig. 14 Failure probability of SiO_2 thin film specimens: (**a**) Weibull model fitted to results and (**b**) lognormal model fitted to results

characteristic strength with the same units as failure strength [25]. Given that a physical basis exists for the strength data to follow a Weibull distribution, this two-parameter model can be used to predict the probability of failure of brittle materials. Size effects for geometries other than straight specimens (e.g., at stress concentrations) can play a role in determining the fracture strength and should be considered in the design of microelectronics and MEMS. A rigorous probabilistic approach, such as reported in [26] for polysilicon, should be undertaken for design of complex geometries.

Alternatively, the failure strengths of brittle materials are sometimes described by a lognormal distribution, where the probability of failure is given by:

$$p_f^{LN} = \frac{1}{2}\left[1 + \mathrm{erf}\left(\frac{\ln(\sigma) - \mu}{s\sqrt{2}}\right)\right] \tag{2}$$

where μ is the mean and s is the standard deviation of the natural log of the strength data [27]. Figure 14 shows the empirical cumulative distribution function of the measured fracture strengths of the SiO_2 samples, along with Weibull (14a) and lognormal (14b) distribution fits to the data. The upper and lower bounds of the 95% confidence intervals for the two fits to the data are also plotted as dashed lines. The data fits yield the following estimated parameters that describe the distributions:

Weibull : $m = 6.7$ and $\sigma_\theta = 387.5$ MPa

Lognormal : $s = 0.15$ and $\mu = 5.9$ with $e^\mu = 365.0$ MPa.

Table 1 Results of measurement of Young's modulus and strength of SiO_2 for this study, along with other published values

Material	Sample thickness	E (GPa)	Fracture strength (MPa)	Test method	Comments	Reference
PECVD	1.0 µm	60.1±3.4 (25 tests)	364±57 (26 tests)	Tensile	Digital imaging	This work
PECVD	0.5 µm	64±7 (20 tests)	365±67 (18 tests)	Tensile	Differential stiffness	[23]
Thermal SiO_2	<2 mm	66		Bulge	Assumed ν= 0.18	[15]
Thermal-wet, thermal-dry, and sputtered SiO_2	0.3–0.4 µm	57–92, COV= ±20%		Resonance	Various depositions	[16]
Thermal SiO_2	1 µm	64		Beam bending		[17]
Thermal SiO_2	1 µm	83	>600	Nano-indentation		[17]
PECVD, LPCVD	1–3 µm	64±2 61±2		Brillouin light scattering	Calculated from thermal stresses	[18]
PECVD	0.5 µm	59		Beam bending	Calculated from thermal stresses	[19]
PECVD	0.5 µm, 2 µm	59–82		Nano-indentation	Various dielectric interlevels	[20]
Thermal SiO_2	0.4 µm	85±13 (12 tests)		Atomic force microscopy	Beam bending	[21]
PECVD	0.65 µm		600–1900	Tensile	Tested in air and vacuum	[22]
Bulk SiO_2		73				[28]

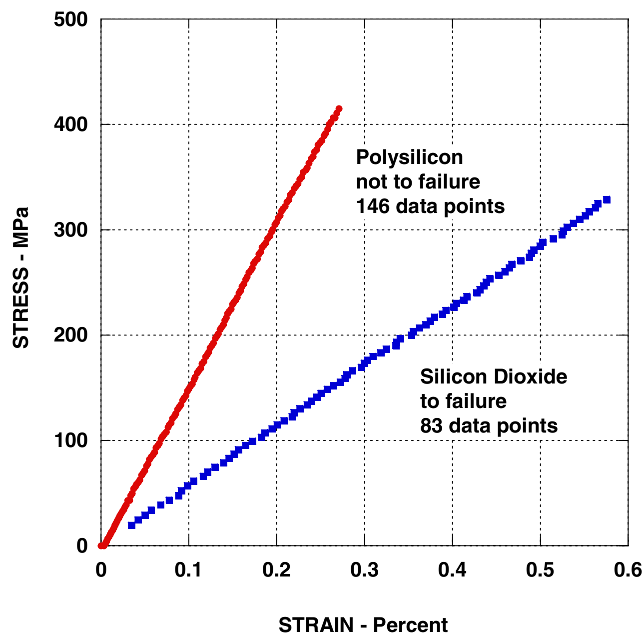

Fig. 15 Comparison of *tensile curves* obtained using two noncontact strain measurement techniques: ISDG (on thin film polysilicon) and image-based (on thin film silicon dioxide)

Table 1 lists the results of mechanical testing of SiO_2 microspecimens using the image-based strain measurement technique alongside the results from other studies of silicon dioxide using a variety of techniques. It can be noted from this table that there are very few studies that report values of the fracture strength of SiO_2 since typically indirect methods of testing are employed, which typically only yield elastic properties.

The coefficient of variation (standard deviation/mean value, or COV) is a useful measure of the relative scatter of data. The modulus COV is 5.7%, and the strength COV is 15.7%. It is interesting to compare these with measurements on bulk materials. Dowling [29], in Table B.4 lists typical COVs for various mechanical properties. The COV for modulus of elasticity is surprisingly high at 5%, which is only slightly better than for these measurements. Strength COVs are 7% for yield and 5% for ultimate. No tensile strength value is given for brittle metals, but the COV for the compressive strength of concrete is 15%. The fact that the variation in results from these microspecimens is similar to that for large specimens supports the validity of this test method.

Concluding Remarks

Table 1 shows that there are remarkably few studies of the mechanical properties of thin film silicon dioxide; given its importance in the microelectronics and MEMS industries. True, it serves mostly as an insulator and not as a deformable structural element, but it does influence the overall mechanical behavior of the complete microdevice. The film thicknesses studied are all within the range of ~0.3–3 μm, and the modulus values are reasonably consistent among the various test methods. Note that only one other study reports the number of specimens tested; it is important to test many samples, particularly if probability theories are to be evaluated. The almost complete absence of strength values is because the other test methods don't have freestanding specimens and force measurements. Tsuchiya's tensile results [22] show a very high value (1.9 GPa) for a material that is presumably similar. From this work, a designer can comfortably use a Young's modulus of 60 GPa and a fracture strength of 365 MPa for vapor-deposited silicon dioxide.

It is also interesting to note that the results of this work and those of an early study of silicon dioxide from the same source [23] are nearly the same. The fracture strengths are identical as would be expected since the gripping and loading techniques are the same. However, the earlier work used differential stiffnesses to determine Young's modulus. That method is subject to larger uncertainties since it involves subtraction of similar numbers, but the COV is only twice that of the DDIT. The conclusion is that differential stiffness works well if one is very careful. It

Table 2 Comparison of ISDG and DDIT

	ISDG	DDIT
Resolution	10 microstrain	100 microstrain
Speed	Realtime at ~2 samples/s	Postprocessed
Scope	Single point strain	Single point here; can be biaxial or full-field
Sensitivity to axial displacement	Little	Can be an issue for large displacements
Sensitivity to normal displacement	Very sensitive	Little
Strain markers	Requires high quality markers as part of manufacture	Markers easily applied after specimen is mounted
Materials and surface preparation	Opaque materials with smooth surface	Any material and surface finish
Ease of use once specimen is mounted	Easy	Easy
Cost of setup-exclusive of computer and programs	~$10K for diode arrays and laser	~$5K for camera and single lens with large working distance.

does take twice as many specimens and does not permit measurement of Poisson's ratio. The DDIT approach could easily be extended for Poisson's ratio measurements by making the specimen gage section wider.

Digital imaging methods–DDIT or digital image correlation (DIC)—are completely different than interferometric methods such as the ISDG. Both can be used to measure mechanical properties of thin films as Fig. 15 shows. The polysilicon film whose results are shown is 3.5 μm thick with a gage section 50 μm wide [30]. It is a strong material with fracture strengths on the order of 1.5 GPa, but only the first part of the stress-strain curve is shown for clarity. The silicon dioxide result is from Fig. 10. The figure shows that both methods give good results; there is sufficient resolution and an adequate number of data points.

There are differences of course, and Table 2 lists them.

The main and obvious difference between the two methods is that the ISDG is realtime and more sensitive. However, it is more sophisticated in its implementation. The DDIT is less complicated, and there are commercial digital imaging programs that can be used. Postprocessing is required, but this will change with advances in computer and camera technology. It is useful to add a displacement measurement with the DDIT so that the operator can monitor the overall deformation of the specimen. The ability of the DDIT to measure a wide variety of materials with little surface preparation is a considerable advantage.

Acknowledgements The authors acknowledge the support of the Sensors and Electron Devices Directorate of the Army Research Laboratory and Dr. Madan Dubey. Ryan McCaffrey, a Mechanical Engineering undergraduate, conducted many of the tests. Professor Lori Graham-Brady assisted with the probability analyses.

References

1. Madou M (1997) Fundamentals of microfabrication. CRC, Boca Raton, FL.
2. May GS, Sze SM (2004) Fundamentals of semiconductor fabrication. Wiley, Hoboken, NJ.
3. Senturia SD (2001) Microsystem design. Kluwer, Norwell, MA.
4. Petersen KE (1982) Silicon as a mechanical material. In: Proceedings of the IEEE, pp 420–457.
5. Sharpe WN Jr. (2001) Mechanical properties of MEMS materials. The MEMS handbook. CRC, Boca Raton, FL, pp 3-1–3-33.
6. Read DT, Dally JW (1992) A new method for measuring the constitutive properties of thin films. J Mater Res 8:1542–1549.
7. Sharpe WN Jr., Yuan B, Edwards RL (1997) A new technique for measuring the mechanical properties of thin films. J Microelectromech Sys 6:193–199.
8. Tsuchiya T, Tabata O, Sakata J, Taga Y (1997) Specimen size effect on tensile strength of surface micromachined polycrystalline silicon thin films. In: Proceedings IEEE tenth annual international workshop on micro electro mechanical systems, pp 529–534.
9. Sharpe WN Jr., Turner KT, Edwards RL (1999) Tensile testing of polysilicon. Exp Mech 39:162–170.
10. Sharpe WN Jr., Jackson K, Coles G, Eby MA, Edwards RL (2001) Tensile tests of various thin films. Mechanical properties of structural thin films, ASTM STP 1413, American Society of Testing and Materials, pp 229–247.
11. Chasiotis I, Knauss WG (2000) Microtensile tests with the aid of probe microscopy for the study of MEMS materials. In: Proceedings of the SPIE, pp 96–103.
12. Espinosa HD, Prorok BC, Peng B (2004) Plasticity size effects in free-standing submicron polycrystalline FCC films subjected to pure tension. J Mech Phys Solids 52:667–689.
13. Haque MA, Saif MTA (2002) In-situ tensile testing of nano-scale specimens in SEM and TEM. Exp Mech 42:123–128.
14. Long GS, Read DT, McColskey JD, Crago K (2001) Microstructural and mechanical characterization of electrodeposited gold films. ASTM STP 1413, American Society of Testing and Materials, pp 262–277.
15. Jaccodine RJ, Schlegel WA (1966) Measurements of strain at Si–SiO_2 interface. J Appl Phys 37:2429–2433.
16. Petersen KE, Guarnieri CR (1979) Young's modulus measurements of thin films using micromechanics. J Appl Phys 50:6761–6766.
17. Weihs TP, Hong S, Bravman JC, Nix WD (1988) Mechanical deflection of cantilever microbeams: a new technique for testing the mechanical properties of thin films. J Mater Res 3:931–942.
18. Carlotti G, Doucet L, Dupeux M (1997) Elastic properties of silicon dioxide films deposited by chemical vapour deposition from tetraethylorthosilicate. Thin Solid Films 296:102–105.
19. Zhao JH, Ryan T, Ho PS (1999) Measurement of elastic modulus, poisson ratio, and coefficient of thermal expansion of on-wafer submicron films. J Appl Phys 85:6421–6424.
20. Chen F, Li B, Sullivan TD, Gonzalez CL, Muzzy CD, Lee HK, Levy MD, Dashiell MW, Kolodzey J (2000) Influence of underlying interlevel dielectric films on extrusion formation in aluminum interconnects. J Vac Sci Technol B 18:2826–2834.
21. Sundararajan S, Bhushan B, Namazu T, Isono Y (2002) Mechanical property measurements of nanocscale structures using an atomic force microscope. Ultramicroscopy 91:111–118.
22. Tsuchiya T, Inoue A, Sakata J (2000) Tensile testing of insulating thin films: humidity effect on tensile strength of SiO_2 films. Sens Actuators, A, Phys 82:286–290.
23. Gianola DS, Sharpe WN Jr. (2004) Techniques for testing thin films in tension. Exp Tech 28:23–27.
24. Sharpe WN Jr., Jackson KM, Hemker KJ, Xie Z (2001) Effect of specimen size on Young's modulus and fracture strength of polysilicon. J Microelectromech Syst 10:317–326.
25. Weibull W (1951) A statistical distribution of wide applicability. J Appl Mech 18:293–297.
26. Bagdahn J, Sharpe WN Jr., Jadaan O (2003) Fracture strength of polysilicon at stress concentrations. J Microelectromech Syst 12:302–312.
27. Holman JP (1989) Experimental methods for engineers. McGraw-Hill, New York, NY.
28. Spearing SM (2000) Materials issues in microelectromechanical systems (MEMS). Acta Mater 48:179–196.
29. Dowling NE (2007) Mechanical behavior of materials. Prentice Hall, New Jersey, Table B.4.
30. Sharpe WN Jr., Eby MA, Coles G (2001) Effect of temperature on mechanical properties of polysilicon. In: Proceedings of transducers, pp 1366–1369.